FISEVIER

Contents lists available at ScienceDirect

Journal of Wind Engineering & Industrial Aerodynamics

journal homepage: www.elsevier.com/locate/jweia





Dynamic properties of an aeroelastic transmission tower subjected to synoptic and downburst-like outflows

Kehinde J. Alawode ^{a,*}, Ziad Azzi ^b, Amal Elawady ^{a,c}, Arindam Gan Chowdhury ^{a,c}

- ^a Department of Civil and Environmental Engineering, Florida International University, Miami, FL, USA
- ^b DDA Forensics, Miami, USA
- ^c Extreme Events Institute of International Hurricane Research Center, Florida International University, Miami, FL, USA

ARTICLE INFO

Keywords: Transmission tower Downburst Aeroelastic Dynamic behaviour High-intensity winds Synoptic winds

ABSTRACT

Electrical transmission towers can be vulnerable to high intensity non-synoptic wind events such as downbursts. This paper compares the wind-induced response of a single self-supported transmission tower subjected to experimentally produced downburst outflows and synoptic (i.e., atmospheric boundary layer (ABL)) winds. Wind tunnel tests were carried out on a 1:50 aeroelastic model of the tower. A similar mean wind speed was produced at 1/6th of tower height and tower height in the downburst and synoptic simulations, respectively. Lower drag coefficients were observed under downburst winds in comparison to synoptic winds for the case tested. Lower peak base shear and base moments were subsequently observed in the downburst case. However, the results indicate that the base dynamic response of a self-supported tower can be slightly higher under downburst wind loads in comparison to synoptic winds. Higher dynamic amplification factors (DAF) and deviations from the mean were observed in the base dynamic response to downburst winds in comparison to the synoptic case. This indicates that self-supported towers can be subjected to more wind-induced vibrations under downburst winds with similar peak wind speeds as the synoptic winds.

1. Introduction

The overhead high-voltage transmission towers are a major part of the power distribution network. Damage to transmission towers within a distribution system can cause power outages that extend to several cities served by this network. With the integration of electricity into daily life, a shortfall in electricity supply can lead to both social and economic losses as evidenced by the billions of dollars of losses associated with the 2021 Texas power outages (Busby et al., 2021). A report by Electric Power Research Institute (EPRI) (Lineweber and McNulty, 2001) estimates that the US economic losses due to power outages are between \$104 and 164 billion annually. Although transmission towers are designed to resist environmental loads including wind loads, inspection of damaged towers have identified failures due to spatially and temporally localized high-intensity wind events such as downbursts (Elawady et al., 2017). Preventing damage to transmission towers due to downbursts is particularly important given the current global rise in rapidly intensifying windstorms (Bhatia et al., 2019; Kossin et al., 2020).

Downburst outflows have non-stationary flow characteristics (Orwig and Schroeder, 2007), shorter duration, and their maximum wind

speeds occur closer to the ground. Hence, they differ from synoptic/atmospheric boundary layer (ABL) winds. This peculiarity has made the analysis of structural loads under downburst winds difficult, and many wind load provisions are unsuitable for analyzing downburst loads on transmission towers. While the new ASCE 74 (2020) guidelines for electrical transmission line (TL) structural loading have some recommendations for downburst loading, more research is necessary to examine their suitability to capture the complex dynamic response of different TLs and to increase the resilience of overhead transmission line systems.

Experimental (Elawady et al., 2017) and numerical (Shehata et al., 2005; Aboshosha and El Damatty, 2015) methods have been used to better understand the impact of downbursts on transmission lines (TLs) primarily because full-scale data collection can be difficult (Aboshosha et al., 2016). Experimental simulations of downbursts in the past have used: i) an impinging jet method (Chay and Letchford, 2002; Elawady et al., 2017) which represents three-dimensional (3D) downburst outflows and ii) a flow redirection method (Butler and Kareem, 2007; Le and Caracoglia, 2019) which constitutes two dimensional (2D) downburst outflows. However, transmission line systems have not been

E-mail addresses: kalaw003@fiu.edu (K.J. Alawode), ziad@ddaclaims.com (Z. Azzi), aelawady@fiu.edu (A. Elawady), chowdhur@fiu.edu (A.G. Chowdhury).

^{*} Corresponding author.

experimentally evaluated in flow-redirected simulations of downburst events, probably due to the small flow section of the currently available downburst simulators. Abd-Elaal et al. (2018) and Aboshosha et al. (2016) give comprehensive reviews of TLs under downburst wind loads.

Unlike synoptic winds, field measurements (Canepa et al., 2020) have shown downburst winds generally have a vertical component due to both the downdraft of air and the primary rolling vortex that causes two main wind components; radial and axial. Mara et al. (2010) assessed the impact of vertical wind vector component on parts of a lattice tower. In comparison to horizontal winds, their study concluded that vertical winds cause higher wind loads for sections with different faces about the vertical axis and higher solidity. This was attributed to an increased projected area in the vertical wind case. The study by Romanic et al. (2021) comparing drag coefficients on circular cylinders under synoptic ABL and downbursts indicated higher values under downburst simulations, although at relatively low Reynolds number between 0.9×10^3 and 1.5×10^4 which is expected to impact the drag coefficient results especially for circular sections. Thus, there could be differences in the aerodynamic coefficients under downburst wind loads for lattice structures. While this variation might not have a significant effect on the entire TLs's response, it might have a local effect on different sections along the tower height or it might influence the response of a single tower during the construction phase. Aerodynamic coefficients are important in effectively predicting the response of the TLs under downburst wind loads and therefore need to be investigated.

Comparisons of structural responses under downburst winds and synoptic winds have been carried out numerically by many researchers. Zhong et al. (2022) found higher dynamic amplification factors (DAF)

under downburst wind loads in comparison to synoptic wind loads at similar mean wind speed, when the ratio of tower height (H) to the vertical position where wind speed is half of the maximum wind speed (δ) is greater than 0.75. Wang et al. (2022) found a reduction in the ratio of base bending moments and tower top peak displacements under downburst wind loads to synoptic winds with increasing tower heights (i.e., 1.45 to 1.01 and 1.18 to 0.91, respectively). Compared to the synoptic case, a 45% increase in base bending moments was observed under downburst wind loads for the shortest tower considered (i.e., 45.5 m). However, these two studies did not consider the influence of the downburst wind direction.

An aeroelastic experimental study was conducted aiming at advancing the knowledge of the dynamic behaviour of electrical transmission lines during downburst events. The downburst testbed used simulates a 2D outflow of downbursts. The produced horizontal velocity profile compares well with the existing field and other laboratory-simulated downbursts. The second section of this paper explains the methodology and the simulator used in this study. The results are analysed and discussed in the third section while the fourth section presents some of the conclusions of the current study.

2. Methodology

2.1. Downburst simulator at the wall of wind

The experimental study was carried out at the United States-National Science Foundation (NSF)-Natural Hazard Engineering Research Infrastructure (NHERI) Wall of Wind (WOW) Experimental Facility (EF) at

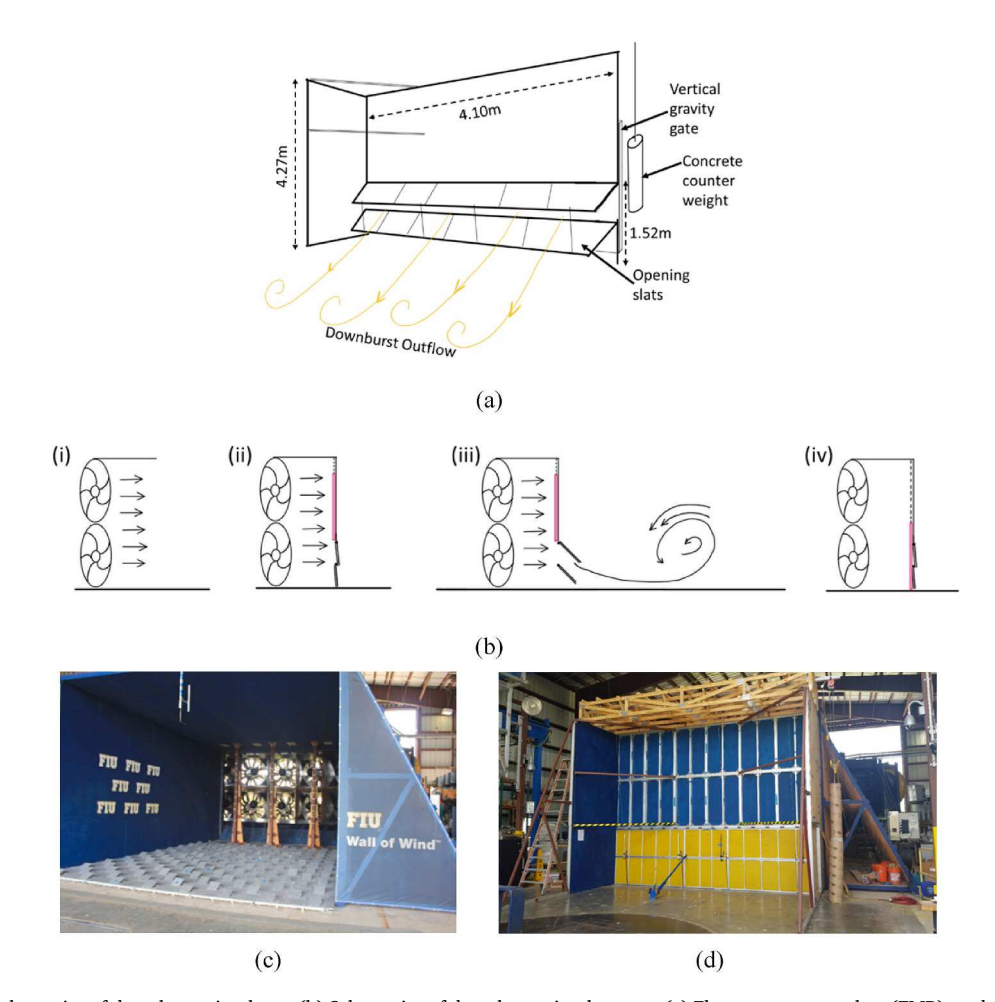


Fig. 1. WOW EF (a) Schematics of downburst simulator, (b) Schematics of downburst simulator use (c) Flow management box (FMB), and (d) Downburst simulator covering the FMB.

Florida International University (FIU). The facility is capable of testing models at wind speeds up to 70 m/s (Gan Chowdhury et al., 2017). The downburst simulator at the facility is a wind re-direction device attached to the outlet of the flow management box of the WOW EF. Mejia et al. (2022) examined different concepts for producing downburst outflows at the WOW. A 2D wall jet concept from that study was incorporated for the WOW. The device has two slats at the lower end which both open to a pre-determined angle and close with the fall of a gravity gate to produce the downburst rolling vortex. Fig. 1 shows the schematics and pictures of the installed downburst simulator on the flow management box (FMB) of the WOW. Its operation follows the steps shown in Fig. 1b (i) Open-Jet facility (ii) Downburst simulator added to FMB, Fan-On, Slats-Closed, Gravity gate-Up (iii) Fan-On, Slats-Open, Gravity gate-Up (iv) Fan-Off, Slats-closed, Gravity gate-Down.

2.2. Wind characteristics

Wind speed and turbulence characteristic measurements at the center of the turntable were measured with Cobra probes sampled at 2500 Hz. The synoptic study simulated an open terrain exposure with a matching velocity profile and turbulence intensity. The downburst velocity profile (shown in Fig. 2) matches the identity of a downburst event where there is a higher wind speed at the lower height with a notable 'nose shape'. Comparisons with the normalized vertical wind profiles of other downbursts in literature also show a similarity. Literature on downburst field events have identified the maximum wind speeds at different heights, some within the first 50 m above ground level (Aboutabikh et al., 2019), others have identified the maximum downburst wind speeds happening between 90 m and 250 m in Europe (Canepa et al., 2020) while a case recorded in Texas, USA reported a maximum wind speed that occurred at 4 m height (Lombardo et al., 2018). In the current study, the maximum wind speed was considered at 4 m full—scale and discussed later. A value of 0.6 s was selected as an appropriate averaging time for the downburst simulation following the approach used by Solari et al. (2015). The decomposition of the wind velocity followed the classical approach shown in Equation (1).

$$U(t) = \overline{U}(t) + U'(t) = \overline{U}(t) + \sigma_U(t)\widetilde{U}'(t)$$
(1)

where U(t) is the wind velocity in the horizontal direction, $\overline{U}(t)$ is the slowly varying mean wind velocity, U(t) is the residual fluctuating wind velocity, $\sigma_U(t)$ is the slowly varying standard deviation of U(t), and $\widetilde{U}(t)$ is the reduced turbulent fluctuation. Fig. 3 shows the time series of wind speed for the synoptic (at 0.55 m height) and downburst (at 0.08 m height) winds, with arrows indicating the peak zone of the record. The ABL study had a test duration of 2 min s but only the first 40 s is shown in Fig. 3. More details about the selection of this peak zone are provided in section 2.4. The mean wind speed within the peak zone was selected as the mean wind speed for the downburst case.

Fig. 4 shows the turbulence intensity of the synoptic and downburst wind simulations. The analysis of turbulence intensity I_u for the downburst is defined in Equation (2).

$$I_{u,T} = E \left[\frac{\sigma_{u(t,z)}}{\overline{U}_{max(t)}} \right]_{T} \tag{2}$$

where $I_{u,T}$ is the time-varying expected value of instantaneous turbulence intensity, $\sigma_{u,(t,z)}$ is the non-stationary slowly varying standard deviation of U(t) at a height z, and $\overline{U}_{max(t)}$ is the maximum $\overline{U}(t)$ across the height. T is set to the experimental sampling rate making it a nearly-instantaneous turbulence intensity. The I_u value presented in Fig. 4a is calculated at each height of the cobra probes within the peak zone (i.e., time range of 9.7s–21.3s). A similar approach was employed by Aboutabikh et al. (2019) where a window of twice the time of the main vortex around the peak velocity was used. Fig. 4b shows a comparison of I_u simulated at the WOW and those reported from other downburst simulators and a field event in Texas on June 19, 2003 (at time of peak wind velocity) as reported by (Lombardo et al., 2018). The plot indicates the I_u in the WOW downburst simulations are within the bounds of other previous studies.

The reduced turbulent fluctuating wind velocity $\widetilde{U}(t)$ from the downburst wind is expected to have a similar characteristic (i.e. Gaussian and stationary) as the synoptic wind velocity (Solari et al., 2015). The power spectral densities (PSD) of both the downburst and synoptic wind simulations are similar and shown in Fig. 5. Statistical

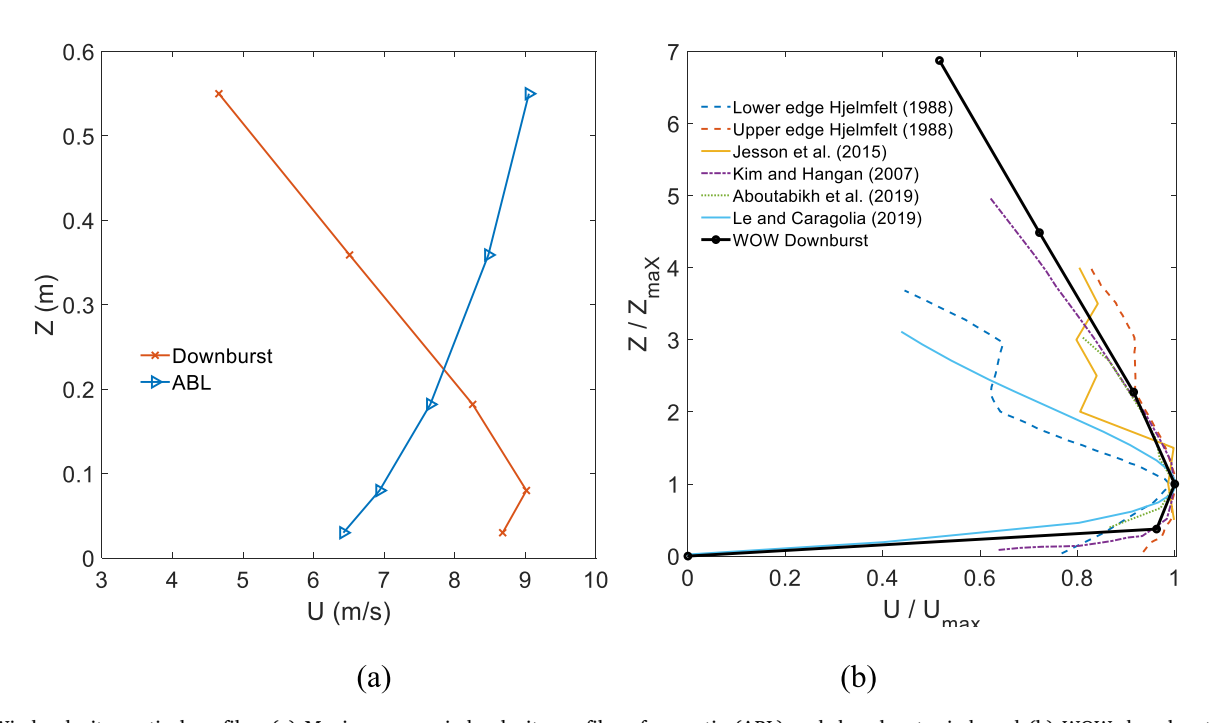


Fig. 2. Wind velocity vertical profiles: (a) Moving-mean wind velocity profiles of synoptic (ABL) and downburst wind, and (b) WOW downburst simulation and others.

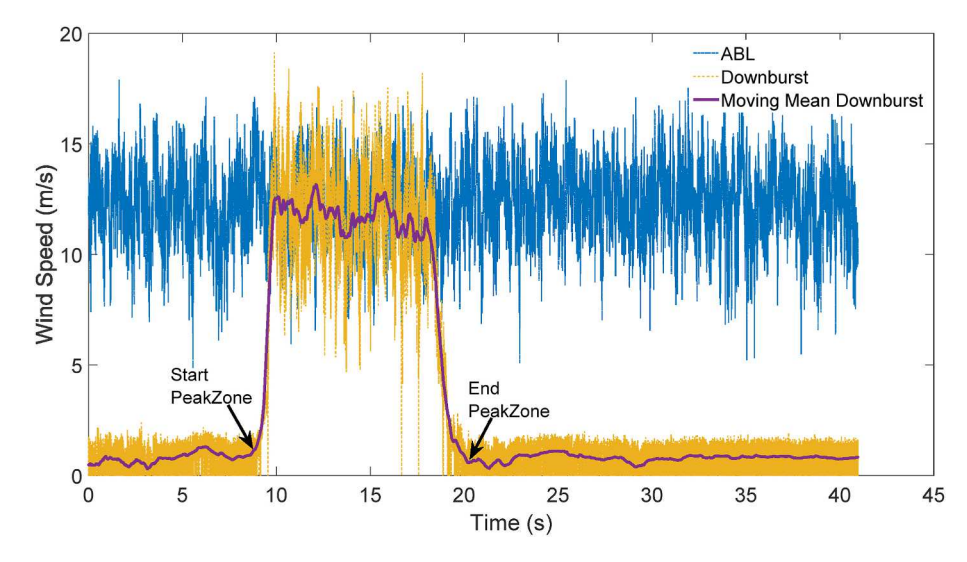


Fig. 3. Time series of Wind speed for the 13 m/s case at 0.08 m height for downburst and 0.55 m height for synoptic winds.

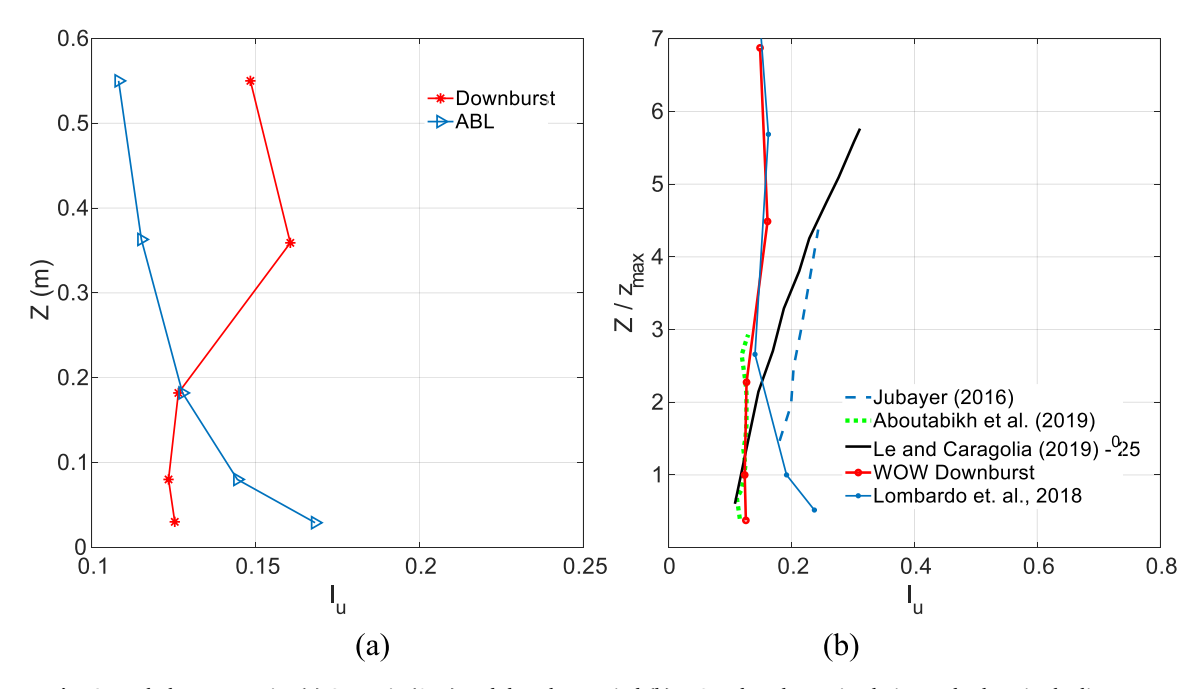


Fig. 4. Turbulence Intensity (a) Synoptic (ABL) and downburst wind (b) WOW downburst simulation and others in the literature.

analysis of a typical $\widetilde{U}(t)$ from the WOW simulation indicates a mean of -0.065, a standard deviation of 1.002, a kurtosis of 3.382 and a skewness of -0.331. These values are close to the expected mean of 0, a standard deviation of 1.0, a kurtosis of 3.0 and a skewness of 0 expected of Gaussian/stationary wind velocity statistics.

2.3. Transmission tower model, instrumentation, and testing protocol

The prototype transmission tower adopted in this study was a steel double circuit vertical self-supported lattice tower with a 7.6 m by 2.7 m base (Length x Width) and 27.5 m height. The natural frequency of the tower in the longitudinal and transverse modes of vibration are 2.25 Hz and 5.10 Hz respectively. Details of the aeroelastic modeling, validation and instrumentation of the model tower can be found in the studies by Azzi et al. (2021, 2022) and Jeddi et al. (2023) which focused on the wind-induced response of the tower to high synoptic winds. The length scale was 1:50 and Table 1 shows the scaling factors used. The

aeroelastic tower has a single spine designed to replicate the dynamic properties of a full-scale tower surrounded by a cladding (attached at 7 zones along the spine) representing the shape of the lattice steel angles of the tower. Three accelerometers, six strain gauges and one 6-DOF load cell were attached to the model tower. Tower responses from these instrumentations were sampled at 500 Hz. Fig. 6 shows a schematic of the tower and the positions of the instrumentations. The tests were run from 0° (wind along the weak axis of the tower) to 90° (strong axis of the tower) wind attack angle at 15° increments, and 8.1 m/s, 9.2 m/s, 10.5m/s and 13 m/s as maximum downburst horizontal wind velocity at 1/6th of the tower height. These wind velocities correspond to the mean wind velocities at tower heights in the synoptic ABL tests by Azzi et al. (2021). In comparing synoptic and downburst wind effects on structures, three approaches are usually followed:(i) Comparing events where the peak wind velocity at the downburst nose matches the wind velocity at tower height (ii) Comparing events where the wind velocity at tower heights under both downburst and synoptic ABL match and (iii)

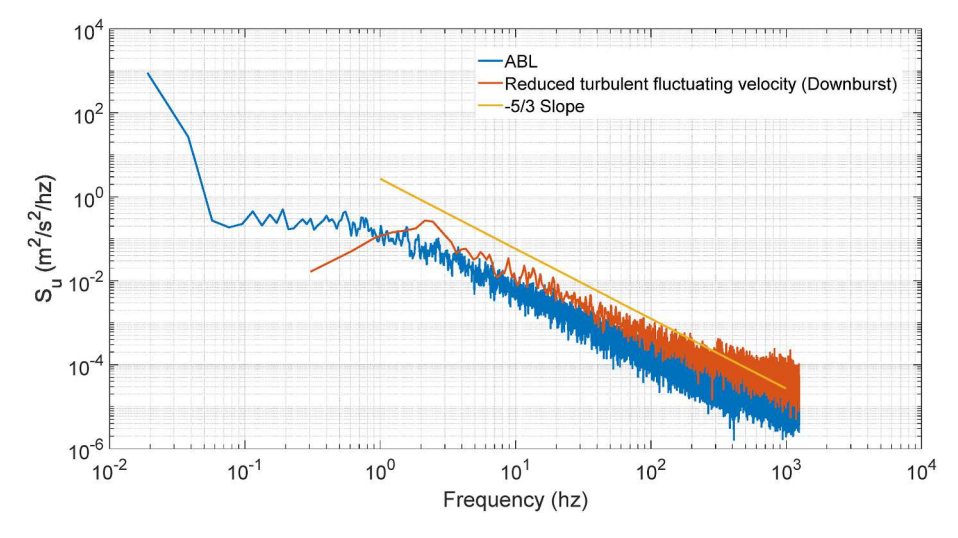


Fig. 5. PSD of Reduced turbulent fluctuating velocity in Downburst and Synoptic/ABL wind velocity.

Table 1 Scaling factors.

Quantity Q	Scaling factor	Quantity	Scaling factor
Length L	1:50	Damping ζ	1:1
Velocity U	1:7.07	Elastic stiffness EI	1:505
Mass m	$1:50^{3}$	Elastic stiffness EA	$1:50^{3}$
Mass moment of inertia I	1:505	Force F	$1:50^{3}$
Time t	1:7.07	Bending moment M	1:504
Acceleration a	1	Torsional moment T	1:504

Comparing events with matching wind velocity at 10 m height. The first approach was used in this study. Table 2 shows the testing protocol indicating wind directions, model scale maximum wind speed at the nose of the downburst profile (i.e., maximum wind speed along tower height) and model scale maximum wind speed at tower height for the ABL study.

2.4. Peak zone selection

A peak zone for the wind velocity, strains, accelerations, base shears, and base moments time histories was selected using the statistical approach for the detection of change-point developed by Lavielle

(2005). This method has also been applied to downburst wind data by Romanic et al. (2019) and Alawode et al. (2022). A change point is a position within the time series records at which the mean or standard deviation of a segment of the time series data change beyond a given threshold. Based on this approach, the peak zone start and end points were identified as indicated in Fig. 3.

3. Results and discussion

3.1. Time history and statistics of tower response

The time history of base shear, base moments and tower top accelerations at a 90° wind direction and 13 m/s downburst wind speed is shown in Fig. 7. The base shear and base moment responses indicate an increase that reflects the arrival of the downburst at the tower location and dissipation as the rolling vortex passes the tower. The time history indicates a significant tower response in the along wind direction (Fx). The across-wind base shear (Fy) is less than the along-wind base shear (Fx). Interestingly, the vertical reaction (Fz) of the tower almost matches the across-wind base shear (Fy) for the case shown in Fig. 7a. The high value of the vertical reaction Fz in comparison to the base shears Fy and Fx highlights the need to have a better understanding of the different turbulence components in field events and compare them with the

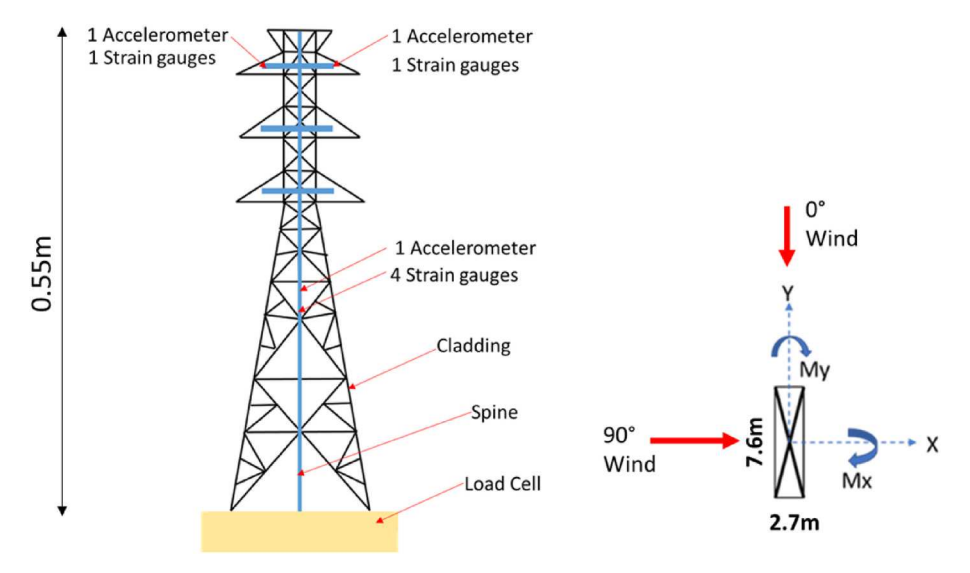


Fig. 6. Schematics of the Tower, Instrumentation and Wind directions.

Table 2
Test protocol.

Test	Wind Directions (°)	Max Wind Speed along tower height (m/s) (Downburst)	Max Wind Speed at tower height (ABL) (m/s)
1	0°, 15°, 30°, 45°, 60°, 75° and 90°	8.1	7.0
2	0°, 15°, 30°, 45°, 60°, 75° and 90°	9.2	9.0
3	0°, 15°, 30°, 45°, 60°, 75° and 90°	10.5	11.0
4	0°, 15°, 30°, 45°, 60°, 75° and 90°	13.0	13.0

simulated ones. Thus, future studies are recommended to assess the effect of the vertical velocity component on the wind actions on lattice towers.

The tower top acceleration time history indicates that the along wind response (Acceleration X) is higher than the across wind response (Acceleration Y) for wind at 90° direction (about 318% higher at peak positions).

The kurtosis and skewness of the acceleration at the tower top are used to examine the Gaussianity of the tower response under synoptic and downburst wind loads. Only responses within the peak zone were considered in the Gaussianity analysis for the downburst case. The kurtosis of a Gaussian process is expected to be 3 while the skewness is expected to be 0 (Zero). Figs. 8 and 9 show the kurtosis and skewness of the acceleration responses respectively for the 90° wind direction under downburst and synoptic wind loads. In both Figs. 8 and 9, U is the fullscale wind speed. Fig. 10 shows the skewness and kurtosis of the tower top acceleration along the Y-axis with the wind direction varying from 0° to 90° at the 9 m/s case. The results indicate that the downburst acceleration responses of the tower are more non-Gaussian in comparison to the synoptic case for both across and along-wind directions. Also, the non-Gaussianity increases with wind speed in the along-wind downburst acceleration response. The 75° wind direction shows the highest non-Gaussain response.

3.2. Tower top accelerations

The root-mean-square (rms) of accelerations on the tower top (cross arms) under the downburst and synoptic ABL wind is presented in

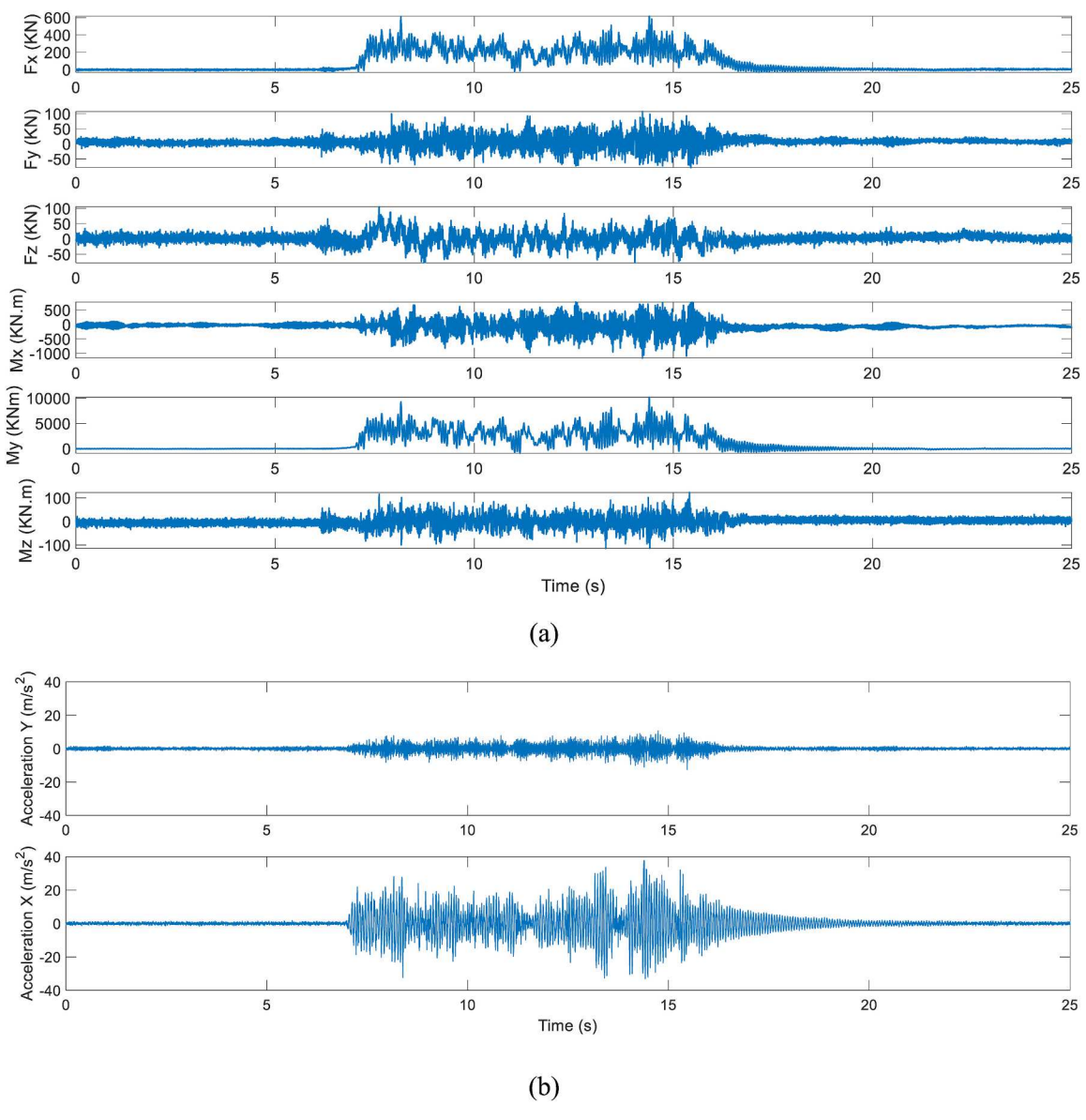


Fig. 7. Response time history samples for 90° Wind direction and 13 m/s (a) Base shear and moments (b) Tower top acceleration.

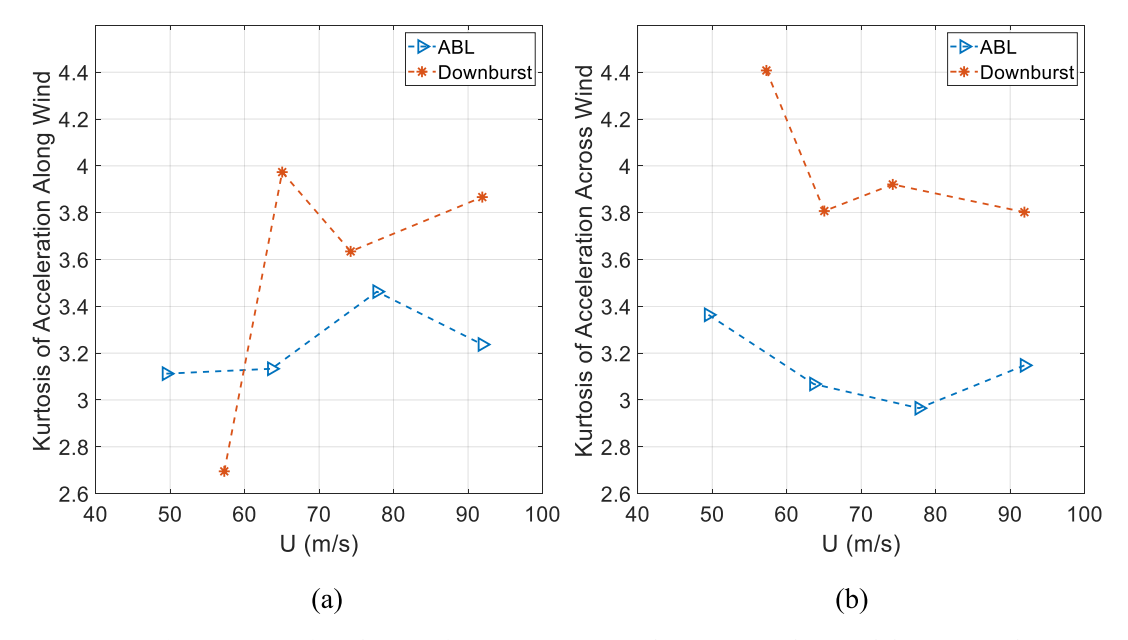


Fig. 8. Kurtosis of Acceleration of Tower Top at 90° Wind Direction (a) Along wind (b) Across wind.

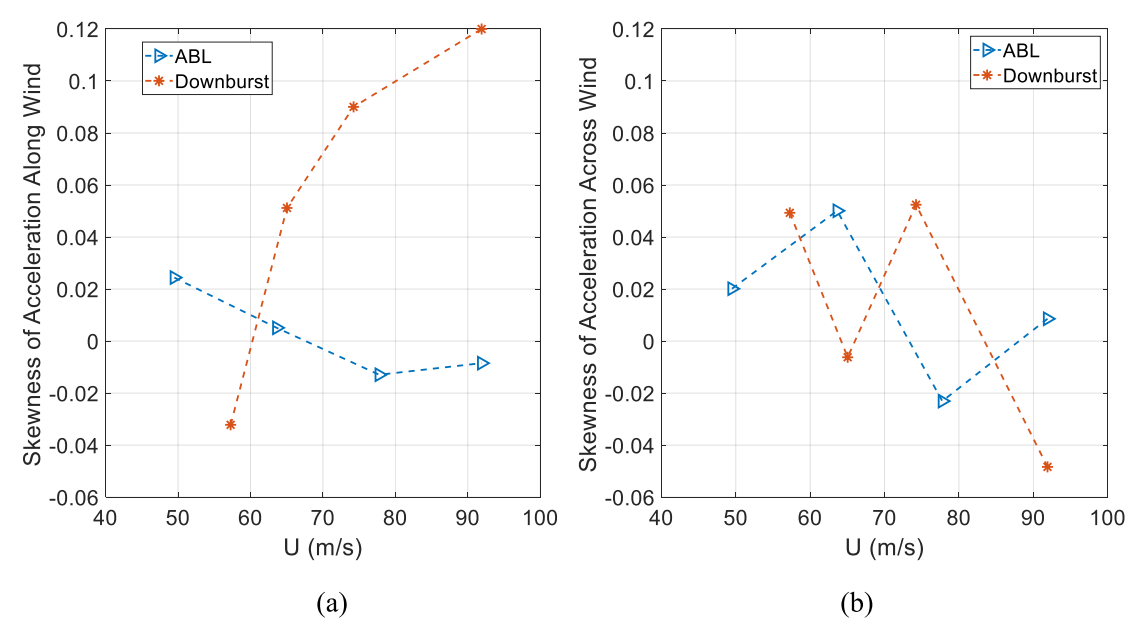


Fig. 9. Skewness of Acceleration of Tower Top at 90° Wind Direction (a) Along wind (b) Across wind.

Fig. 11. Note that U/n•B is the normalized velocity. U is the wind speed at the tower height for the ABL cases, and the wind speed at the downburst nose for the downburst cases. The natural frequency of the tower in Hz is represented by n (i.e., 15.9 Hz along the weak axis of the tower and 35.9 Hz along the strong axis at model-scale). Also, B is the width of the tower at mid-height in m (i.e., 10 cm along the wider face and 4 cm along the narrow face at model-scale). These rms calculations for the downburst event were based on the tower accelerations within the peak zone. Current results show similar acceleration rms at 0° but higher acceleration rms at 90° wind direction under downburst winds in comparison to the ABL winds. The higher acceleration rms values under downburst wind loads in comparison to synoptic winds at 90° wind direction could be because of the larger frontal area in this wind direction. The increase in the downburst-induced accelerations rms

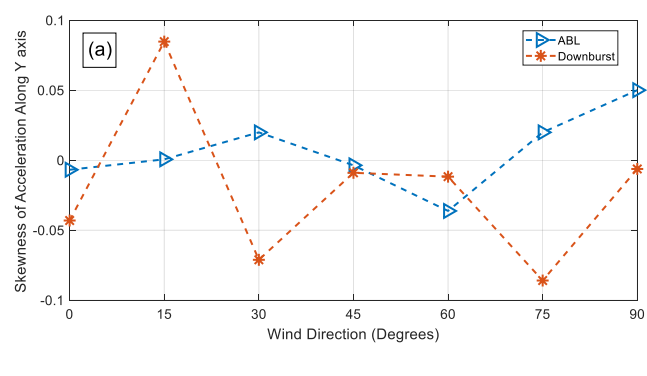
indicates a possible increase in the dynamic response factors. Further studies to confirm these findings are needed.

3.3. Drag coefficients

Theoretically, the drag coefficient C_D is the mean drag force F_D divided by the dynamic pressure (product of half, wind speed U, and density of air ρ) and projected area A as shown in Equation (3).

$$C_D = \frac{F_D}{0.5\rho U^2. A} \tag{3}$$

The measured bending moment M, at the location of the 4 strain gauges (as shown in Fig. 6) can be estimated by a sum of the product of drag forces at each cladding zone F_{Di} and the distance to the strain gauge



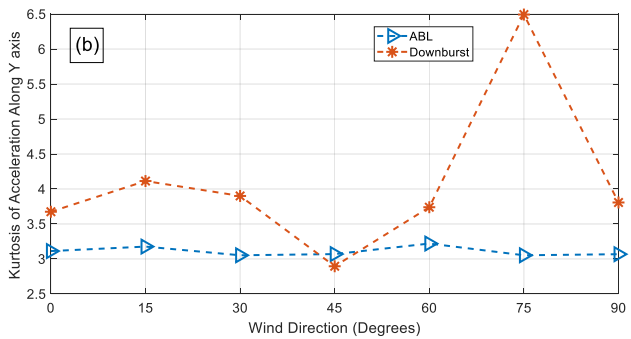


Fig. 10. (a)Skewness of Tower top acceleration along Y axis (b) Kurtosis of Tower top acceleration along Y axis.

location d_i , as shown in Equation (4).

$$M = \sum_{i=1}^{5} F_{Di}.d_i = 0.5.\rho.C_D \sum_{i=1}^{5} A_i.U_i^2.d_i$$
 (4)

Where, U_i is the maximum time-averaged velocity within the peak zone at the height of zone i and A_i is the area of the elements of the tower in the plane perpendicular to the wind direction of zone i (same values from the synoptic tests). The Hooke's law relationship between the strain ϵ and measured bending moment M shown in Equation (5) can be combined with Equation (4) to give an experimental formula for the calculation of C_D .

$$\epsilon = \frac{M.b}{2E.I} \tag{5}$$

This is expressed in Equation (6) (Azzi et al., 2021).

$$C_D = \frac{4 \cdot \epsilon \cdot E \cdot I}{b \cdot \rho \cdot \sum_{i=1}^5 A_i \cdot U_i^2 \cdot d_i}$$
 (6)

where ϵ is the maximum time-averaged strain within the peak zone in the direction of the loading, E is the modulus of elasticity of the spine, E is the moment of inertia of the section about the axis of bending, E is the distance to the centroid, and details of the tower zoning are fully explained in Azzi et al. (2021). Fig. 12 shows a plot of the drag coefficient of the tower under synoptic ABL and downburst winds at varying wind directions. Aside from the E0° wind direction which showed a similar drag coefficient value, drag coefficients are lower (20–48% reduction) in the downburst wind loading case in comparison to the synoptic ABL test. This could be due to the higher turbulence intensity at the upper sections of the tower in the downburst case that yielded to a reduced mean drag force. Zhang et al. (2022) also showed lower E0 in transmission towers subjected to category-B wind fields in comparison to uniform flows.

3.4. Base shears and base moments

The tower response measured by the instrumentation on the tower under wind action is the total response, and it comprises of the mean response and the fluctuating response. The fluctuating response is assumed to be driven by the fluctuating part of the wind action and comprises of the background and resonant response. Elawady et al. (2017) proposed a 7-step methodology for the decomposition of tower responses under downburst wind action which was followed in this analysis.

The decomposition of a sample of base shear response into mean, background and resonant response is shown in Fig. 13. The standard deviation of base shears (std $_{\rm f}$) and base moments (std $_{\rm m}$) of the tower under downburst and synoptic ABL winds at 0° and 90° wind direction is shown in Fig. 14. The results indicate higher standard deviations in base shear forces and base moments under downburst wind loads in comparison to synoptic wind loads for the cases tested.

The observed peak base shear and peak base moments of the tower under downburst and synoptic wind loads at 78 m/s full-scale and

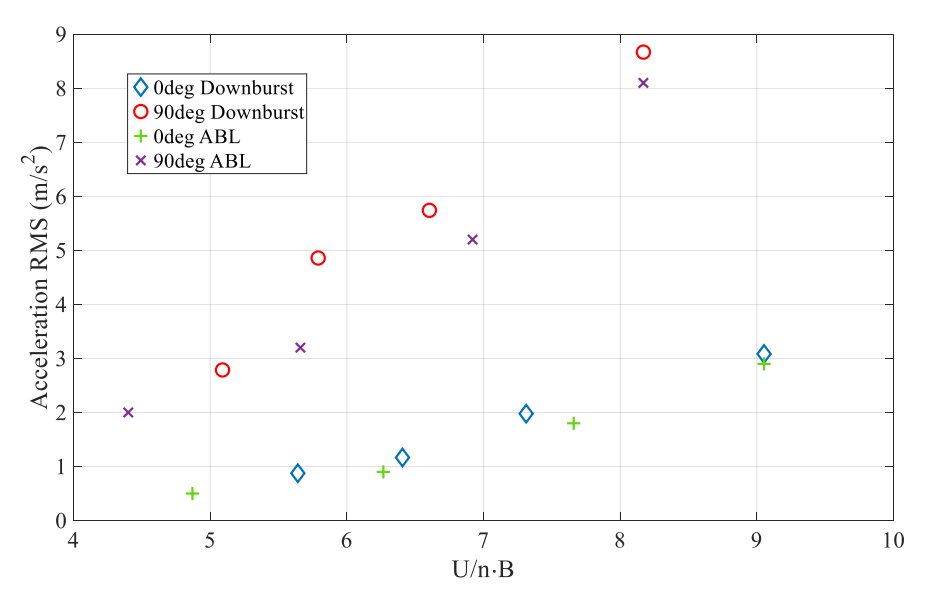


Fig. 11. Tower top acceleration RMS.

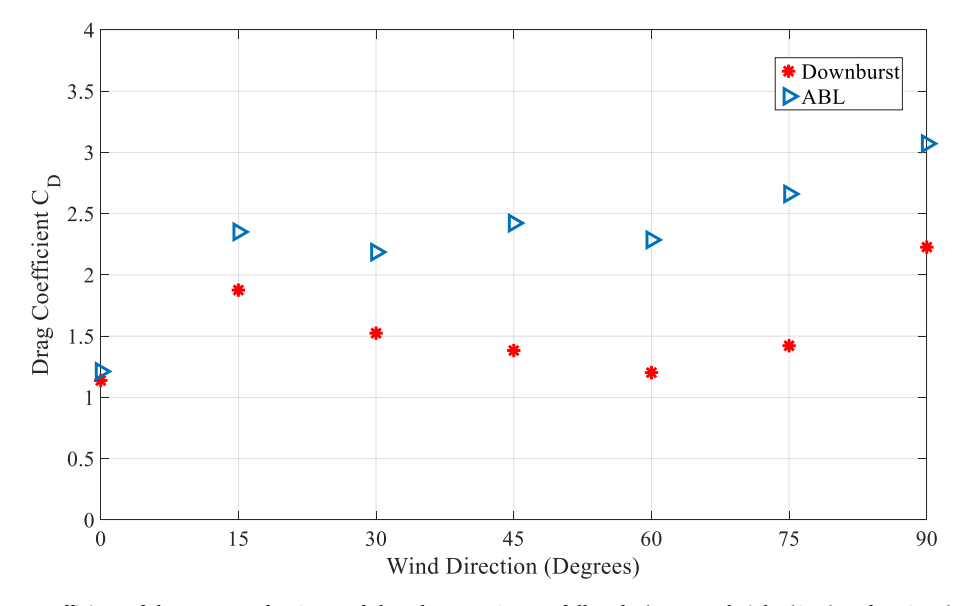


Fig. 12. Drag coefficient of the tower under ABL and downburst at 65 m/s full-scale (at tower height (ABL) and at 4 m (Downburst)).

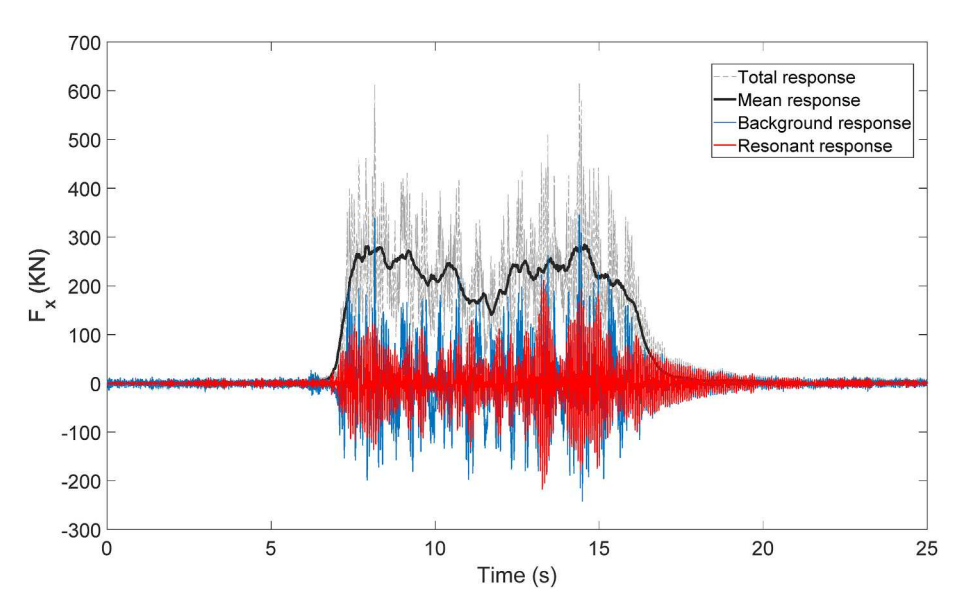


Fig. 13. Total, mean and fluctuating base shear response of tower.

different wind directions are shown in Fig. 15a and b. The results indicate mostly higher values of peak base shear and base moment at all wind directions for the synoptic wind case in comparison to the downburst case except at 0° . The 75° wind direction shows the most difference, with bending moments along y-axis. In both cases of downburst and synoptic wind loading, the maximum base shear and moments occur at 0° and 90° .

3.5. Dynamic amplification factors

Dynamic amplification factor (DAF) is the ratio of dynamic response to quasi-static response, which is often used to account for dynamic effects in a static structural analysis. The higher the DAF values, the higher the dynamic effects. DAF values were calculated after decomposing the response time history into quasi-steady background response and resonant response using the formula given in Equation (7). The quasi-steady background response is a sum of the mean response and the background response.

$$DAF = \frac{\widehat{R}}{\overline{R} + R_{B}} \tag{7}$$

where \widehat{R} is the maximum peak response, \overline{R} is the mean response, and R_B is the background response. To compute the DAF values, the authors used the methodology laid out in Elawady et al. (2017) and Azzi et al. (2021). The DAF estimations used the entire time history of responses under both synoptic and downburst winds. Table 3 shows the DAF at 0° and 90° for both downburst and synoptic wind loads on the tower for the velocity bounds (i.e., at V = 57.3 m/s (Downburst)/49.5 m/s (ABL), and V = 92 m/s (Both Downburst and ABL)). The DAF ranges between 1.03 to 1.28 and 1.07 to 1.16 for base moments and base shear for the downburst case, respectively. The DAF ranges between 1.01 to 1.18 and 1.06 to 1.15 for base moments and base shear for the synoptic case, respectively. The DAF values have a similar trend for both the downburst and synoptic wind loads except for the base shear along 90° . Also, the DAF of base moments along 90° is significantly higher in the downburst wind loading case in comparison to the synoptic wind

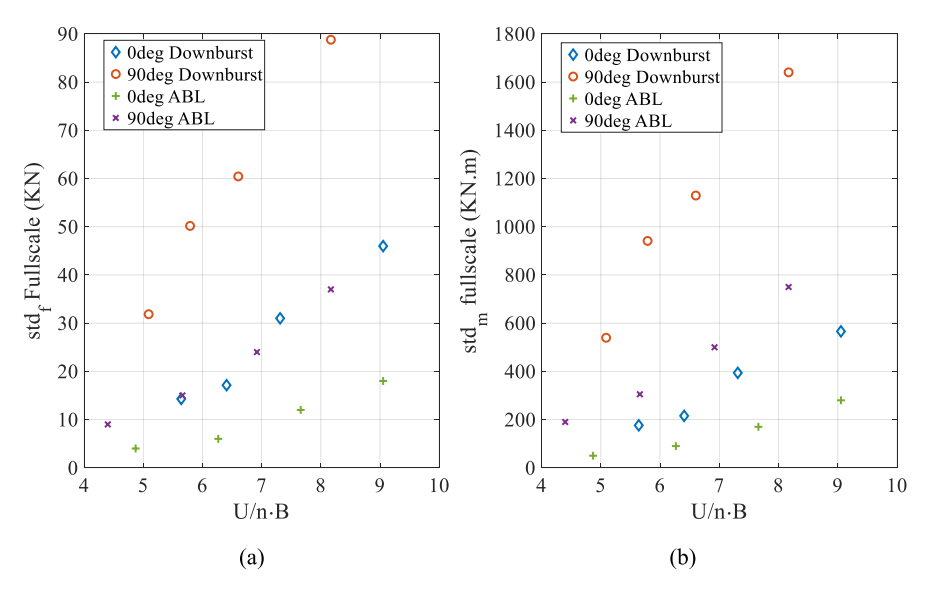


Fig. 14. Standard deviation of full-scale (a) base shears and (b) base moments of the tower.

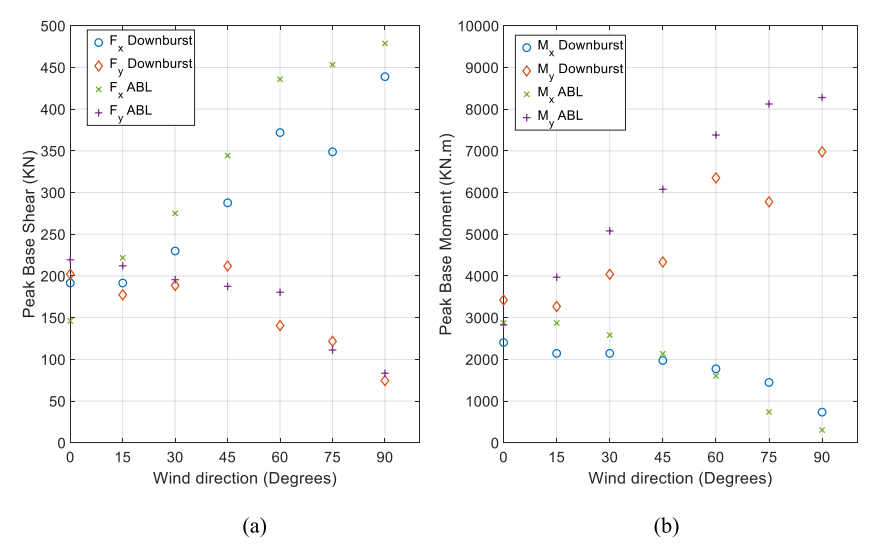


Fig. 15. Peak Base Shear and Base Moments at 78 m/s full scale.

Table 3 DAF analysis.

Wind Direction	Measurement		DAF		Trend
			V = 57.3/ 49.5 m/s	V = 92 m/s	
Along wind	Base	ABL	1.01	1.05	Increasing
0 °	moment	Downburst	1.08	1.12	Increasing
	Base shear	ABL	1.10	1.06	Decreasing
		Downburst	1.15	1.07	Decreasing
Along wind	Base	ABL	1.13	1.18	Increasing
90°	moment	Downburst	1.03	1.28	Increasing
	Base shear	ABL	1.15	1.11	Decreasing
		Downburst	1.12	1.16	Increasing

loading case. The noted difference could be due to the higher projected area at low heights in this wind direction, coupled with the higher wind speeds at low heights for the downburst case.

4. Conclusions

The current study on a self-supported aeroelastic lattice transmission tower has compared the tower response given a matching wind velocity at tower height under synoptic winds and 1/6th tower height under downburst winds. While there is no generally accepted convention for this comparison and given the non-stationarity of downburst events, this study has compared peak zone structural response under downburst winds with the entire time series of structural responses under the synoptic wind. The effect of the difference in event duration was not considered, as it was assumed to have negligible effect on the accuracy of the results. More studies are needed to verify this assumption. Also, this study assumed matching the maximum moving mean downburst wind speed with the mean synoptic wind speed was a basis for comparing tower responses in both scenarios.

The study has shown that the peak dynamic response of a selfsupporting tower can be slightly higher under downburst wind loads in comparison to synoptic wind loads, evidenced by the higher acceleration rms, the higher standard deviation of base shear and base moments and higher DAFs. Also, the tower responses are more non-Gaussian under downburst wind loads in comparison with synoptic wind load responses.

While observed peak responses are presented here for tower responses to both synoptic and downburst winds, further studies showing the distribution of the peak responses in both downburst and synoptic winds would be important. A peak estimation method for non-gaussian structural response can be applied in the future. Also, more studies would be required to assess the observations for other lattice tower types.

Drag coefficients of the single self-supported transmission tower were mostly lower under downburst wind loads in comparison to ABL wind loads. The lower drag and lower wind speed at the tower top resulted in the lower observed peak base shear and base moments observed under downburst loading.

However, more assessment of the adequacy of the quasi-steady analysis applied to tower response data under downburst winds is needed. It would also be important to assess the buffeting response and vortex-shedding-induced dynamic response both across and along wind directions. A framework for comparing wind loads on lattice structures in downburst and synoptic ABL requires further attention.

More tests are planned at the WOW EF for single towers and TLs under downburst loads to consider the effects of varying heights of peak downburst wind speeds on tower response.

Declaration of competing interest

The authors declare the following financial interests/personal relationships which may be considered as potential competing interests: Amal Elawady and Arindam Gan Chowdhury reports financial support was provided by National Science Foundation.

Acknowledgements

These tests were conducted at the NHERI Wall of Wind Experimental Facility (NSF Award No. 1520853 and No. 2037899). This paper is based on work sponsored by NSF under Award No. 1762968. The opinions, findings or conclusions expressed in this article are solely those of the authors and do not represent the opinions of the funding agencies.

References

- Abd-Elaal, E.S., Mills, J.E., Ma, X., 2018. A review of transmission line systems under downburst wind loads. J. Wind Eng. Ind. Aerod. 179, 503–513. https://doi.org/ 10.1016/j.jweia.2018.07.004.
- Aboshosha, H., El Damatty, A., 2015. Engineering method for estimating the reactions of transmission line conductors under downburst winds. Eng. Struct. 99, 272–284. https://doi.org/10.1016/j.engstruct.2015.04.010.
- Aboshosha, H., Elawady, A., El Ansary, A., El Damatty, A., 2016. Review on dynamic and quasi-static buffeting response of transmission lines under synoptic and non-synoptic winds. Eng. Struct. 112. 23–46. https://doi.org/10.1016/j.engstruct.2016.01.003.
- Aboutabikh, M., Ghazal, T., Chen, J., Elgamal, S., Aboshosha, H., 2019. Designing a blade-system to generate downburst outflows at boundary layer wind tunnel. J. Wind Eng. Ind. Aerod. 186, 169–191. https://doi.org/10.1016/j. iweja.2019.01.005.
- Alawode, K.J., Elawady, A., Shafieezadeh, A., Chowdhury, A., 2022. Aeroelastic testing to examine the dynamic behavior of a single self-supported electrical transmission tower subjected to downburst wind loads. Lubbock, TX, USA. In: Proceedings of the 14th Americas Conference on Wind Engineering, pp. 17–19. May 2022.
- ASCE 74, 2020. Fourth, Issue 74. In: Agnew, F. (Ed.), Guidlines for Electrical Transmission Line Structural Loading. American Society of Civil Engineers. https://doi.org/10.1061/9780784415566 (ASCE).
- Azzi, Z., Elawady, A., Irwin, P., Chowdhury, A.G., Shdid, C.A., 2021. Aeroelastic modeling to study the wind-induced response of a self-supported lattice tower. Eng. Struct. 245, 112885 https://doi.org/10.1016/j.engstruct.2021.112885.

- Azzi, Z., Elawady, A., Irwin, P., Chowdhury, A.G., Shdid, C.A., 2022. Aeroelastic modeling to investigate the wind - induced response of a multi - span transmission lines system. Wind Struct. 2, 231–257.
- Bhatia, K.T., Vecchi, G.A., Knutson, T.R., Murakami, H., Kossin, J., Dixon, K.W., Whitlock, C.E., 2019. Recent increases in tropical cyclone intensification rates. Nat. Commun. 10 (1), 1–9. https://doi.org/10.1038/s41467-019-08471-z.
- Busby, J.W., Baker, K., Bazilian, M.D., Gilbert, A.Q., Grubert, E., Rai, V., Rhodes, J.D., Shidore, S., Smith, C.A., Webber, M.E., 2021. Cascading risks: understanding the 2021 winter blackout in Texas. Energy Res. Social Sci. 77, 102106 https://doi.org/ 10.1016/i.erss.2021.102106.
- Butler, K., Kareem, A., 2007. Physical and numerical modeling of downburst generated gust fronts. In: Proceedings of the 12th International Conference on Wind Engineering, pp. 791–798. Cairns, Australia.
- Canepa, F., Burlando, M., Solari, G., 2020. Vertical profile characteristics of thunderstorm outflows. J. Wind Eng. Ind. Aerod. 206 https://doi.org/10.1016/j. iweja 2020 104332.
- Chay, M.T., Letchford, C.W., 2002. Pressure distributions on a cube in a simulated thunderstorm downburst - Part A: stationary downburst observations. J. Wind Eng. Ind. Aerod. 90 (7), 711–732. https://doi.org/10.1016/S0167-6105(02)00158-7.
- Elawady, A., Aboshosha, H., El Damatty, A., Bitsuamlak, G., Hangan, H., Elatar, A., 2017. Aero-elastic testing of multi-spanned transmission line subjected to downbursts. J. Wind Eng. Ind. Aerod. 169, 194–216. https://doi.org/10.1016/j. iweia.2017.07.010
- Gan Chowdhury, A., Zisis, I., Irwin, P., Bitsuamlak, G., Pinelli, J.P., Hajra, B., Moravej, M., 2017. Large-scale experimentation using the 12-fan wall of wind to assess and mitigate hurricane wind and rain impacts on buildings and infrastructure systems. J. Struct. Eng. 143 (7) https://doi.org/10.1061/(ASCE)ST.1943-541X.0001785.
- Jeddi, A.B., Azzi, Z., Shafieezadeh, A., Elawady, A., Chowdhury, A., Irwin, P., 2023. Revisit of underestimated wind drag coefficients and gust response factors of lattice transmission towers based on aeroelastic wind tunnel testing and multi-sensor data fusion. Eng. Struct. 278, 115486 https://doi.org/10.1016/j.engstruct.2022.115486.
- Kossin, J.P., Knapp, K.R., Olander, T.L., Velden, C.S., 2020. Global increase in major tropical cyclone exceedance probability over the past four decades. Proc. Natl. Acad. Sci. U.S.A. 117 (22) https://doi.org/10.1073/pnas.1920849117.
- Lavielle, M., 2005. Using penalized contrasts for the change-point problem. Signal Process. 85 (8), 1501–1510. https://doi.org/10.1016/j.sigpro.2005.01.012.
- Le, V., Caracoglia, L., 2019. Generation and characterization of a non-stationary flow field in a small-scale wind tunnel using a multi-blade flow device. J. Wind Eng. Ind. Aerod. 186, 1–16. https://doi.org/10.1016/j.jweia.2018.12.017.
- Lineweber, D., McNulty, S., 2001. The cost of power disturbances to industrial and digital economy companies. In: EPRI (Issue 3002000476.
- Lombardo, F.T., Mason, M.S., de Alba, A.Z., 2018. Investigation of a downburst loading event on a full-scale low-rise building. J. Wind Eng. Ind. Aerod. 182, 272–285. https://doi.org/10.1016/j.jweia.2018.09.020.
- Mara, T.G., Galsworthy, J.K., Savory, E., 2010. Assessment of vertical wind loads on lattice framework with application to thunderstorm winds. Wind Struct. Int. J. 13 (5), 413–431. https://doi.org/10.12989/was.2010.13.5.413.
- Mejia, A.D., Elawady, A., Vutukuru, K.S., Chen, D., Chowdhury, A.G., 2022. Examination of different wall jet and impinging jet concepts to produce large-scale downburst outflow. Front. Built Environ. 8, 1–21. https://doi.org/10.3389/fbuil.2022.980617.
- Orwig, K.D., Schroeder, J.L., 2007. Near-surface wind characteristics of extreme thunderstorm outflows. J. Wind Eng. Ind. Aerod. 95 (7), 565–584. https://doi.org/ 10.1016/j.jweja.2006.12.002.
- Romanic, D., Ballestracci, A., Canepa, F., Solari, G., Hangan, H., 2021. Aerodynamic coefficients and pressure distribution on two circular cylinders with free end immersed in experimentally produced downburst-like outflows. Adv. Struct. Eng. 24 (3), 522–538. https://doi.org/10.1177/1369433220958763.
- Romanic, D., Chowdhury, J., Chowdhury, J., Hangan, H., 2019. Investigation of abrupt changes in thunderstorm velocity record. Beijing, China September. In: 15th International Conference on Wind Engineering, 2012, pp. 13–16.
- Shehata, A.Y., El Damatty, A.A., Savory, E., 2005. Finite element modeling of transmission line under downburst wind loading. Finite Elem. Anal. Des. 42 (1), 71–89. https://doi.org/10.1016/j.finel.2005.05.005.
- Solari, G., Burlando, M., De Gaetano, P., Repetto, M.P., 2015. Characteristics of thunderstorms relevant to the wind loading of structures. Wind Struct. Int. J. 20 (6), 763–791. https://doi.org/10.12989/was.2015.20.6.763.
- Wang, Z., Yang, F., Wang, Y., Fang, Z., 2022. Study on wind loads of different height transmission towers under downbursts with different parameters. Buildings 12 (2), 193. https://doi.org/10.3390/buildings12020193.
- Zhang, W., Xiao, Y., Li, C., Zheng, Q., Tang, Y., 2022. Wind load investigation of self-supported lattice transmission tower based on wind tunnel tests. Eng. Struct. 252, 113575 https://doi.org/10.1016/j.engstruct.2021.113575.
- Zhong, Y., Li, S., Jin, W., Yan, Z., Liu, X., Li, Y., 2022. Frequency domain analysis of alongwind response and study of wind loads for transmission tower subjected to downbursts. Buildings 12 (2). https://doi.org/10.3390/buildings12020148.